Journal of Sound and Vibration 330 (2011) 788–804

Contents lists available at ScienceDirect

Journal of Sound and Vibration

journal homepage: www.elsevier.com/locate/jsvi

Free vibration of two elastically coupled rectangular plates with uniform elastic boundary restraints

Jingtao Du [a], Wen L. Li [b], Zhigang Liu [a,*], Tiejun Yang [a], Guoyong Jin [a]

[a] College of Power and Energy Engineering, Harbin Engineering University, Harbin 150001, PR China
[b] Department of Mechanical Engineering, Wayne State University, 5050 Anthony Wayne Drive, Detroit, MI 48202-3902, USA

ARTICLE INFO

Article history:
Received 22 August 2010
Accepted 29 August 2010
Handling Editor: L.G. Tham
Available online 24 September 2010

ABSTRACT

An analytical method is derived for determining the vibrations of two plates which are generally supported along the boundary edges, and elastically coupled together at an arbitrary angle. The interactions of all four wave groups (bending waves, out-of-plane shearing waves, in-plane longitudinal waves, and in-plane shearing waves) have been taken into account at the junction via four types of coupling springs of arbitrary stiffnesses. Each of the transverse and in-plane displacement functions is expressed as the superposition of a two-dimensional (2-D) Fourier cosine series and several supplementary functions which are introduced to ensure and improve the convergence of the series representation by removing the discontinuities that the original displacement and its derivatives will potentially exhibit at the edges when they are periodically expanded onto the entire x–y plane as mathematically implied by a 2-D Fourier series. The unknown expansions coefficients are calculated using the Rayleigh–Ritz procedure which is actually equivalent to solving the governing equation and the boundary and coupling conditions directly when the assumed solutions are sufficiently smooth over the solution domains. Numerical examples are presented for several different coupling configurations. A good comparison is observed between the current results and the FEA models. Although this study is specifically focused on the coupling of two plates, the proposed method can be directly extended to structures consisting of any number of plates.

1. Introduction

The vibrations and power flows between two coupled plates are of interest to both researchers and application engineers. A good understanding of the interactions between two plates will provide insight into the design of more complex dynamic systems such as ship hulls, land and space vehicles, and building structures. Although this kind of problems can be easily solved by a numerical method such as FEA, an analytical approach, whenever available, may be preferred because it is typically more suitable for parametric study, sensitivity and uncertainty analysis, and design optimization. In addition, for the same spatial resolution, the number of degrees of freedom is usually much smaller in an analytical model which becomes particularly attractive for high frequency analysis. This is probably why analytical approaches have received a lot of attention for many years.

* Corresponding author. Tel.: +86 451 82518264; fax: +86 451 82569458.
E-mail address: zgliu56@yahoo.com.cn (Z. Liu).

0022-460X/$ - see front matter © 2010 Elsevier Ltd. All rights reserved.
doi:10.1016/j.jsv.2010.08.044

Nomenclature

a length of plate
b width of the plate
D flexural rigidity
E Young's modulus
G extensional rigidity
h thickness of plate
$\mathbf{K}$ stiffness matrix
K_{bx10}, K_{bx11} rotational stiffnesses for bending vibration at $x_1=0$ and a_1, respectively
K_{by10}, K_{by11} rotational stiffnesses for bending vibration at $y_1=0$ and b, respectively
K_{bx10}, K_{bx11} translational stiffnesses for bending vibration at $x_1=0$ and a_1, respectively
K_{by10}, K_{by11} translational stiffnesses for bending vibration at $y_1=0$ and b, respectively
k_{nx10}, k_{nx11} normal stiffnesses for in-plane vibration at $x_1=0$ and a_1, respectively
k_{ny10}, k_{ny11} normal stiffnesses for in-plane vibration at $y_1=0$ and b, respectively
k_{px10}, k_{px11} tangential stiffnesses for in-plane vibration at $x_1=0$ and a_1, respectively
k_{py10}, k_{py11} tangential stiffnesses for in-plane vibration at $y_1=0$ and b, respectively
K_c rotational coupling stiffness at the common edge
k_{c1}, k_{c2}, k_{c3} linear coupling stiffnesses at the common edge in z_1, x_1, y_1-directions, respectively
$\mathbf{M}$ mass matrix
$u(x, y)$ in-plane displacement component in the x-direction
$v(x, y)$ in-plane displacement component in the y-direction
$w(x, y)$ bending displacement in the z-direction
μ Poisson ratio
ρ mass density of plate material
ω angular frequency

In the early investigations, the coupling was typically considered only between the bending waves [1–3]. However, the exclusion of in-plane modes may lead to significant prediction errors at high frequencies, for thick structural components, or at distances far away from the sources [4,5]. Take the ship environment for an example, in which the coupled plates are classical structural form, some phenomenon with onboard machinery like pump cavitation will generate such high frequency vibration. Then, the in-plane resonant modes which are commonly of much higher frequency (usually, up to thousands of Hz) will be easily excited by the transverse motion propagating from its adjacent plate structure for an angled connecting configuration. The in-plane vibrations have been routinely considered nowadays to better predict the dynamic behaviors of and the power flows between two plates coupled together at an angle. In addition to the well-known numerical methods such as the statistical energy analysis method [6–8] and finite element methods [9–11], several analytical methods have been employed to study the vibrational energy flows between coupled plates. Based on the wave description of displacement fields, the power transmissions were studied between semi-infinite plates for various types of joints [12–15]. The dynamic stiffness matrix technique developed by Langley [16] is extended to include in-plane vibrations and applied to ship foundation and hull represented by a row of panels coupled together [17,18]. Cuschieri and McCollum [2,3,19] presented a mobility power flow method to examine the energy transfer through an L-shaped junction. The technique which has been most widely used in the literature for studying the power flows in plate structures is the receptance technique originally proposed by Azimi et al. [20]. Dimitriadis and Pierce [21] employed this technique to derive the energy flows between two plates. Farag and Pan [22] analyzed effects of the coupling angle on the input power and power flow across the coupling edge by using the concept of receptance. Kim et al. [23] extended the method to the interactions of any number of plates at a common junction. The receptance approach was also used by Beshara and Keane [24] to study the energy flows through compliant and dissipative couplings where the response of each substructure is described in terms of Green functions. The interactions between flexural and in-plane vibrations are often ignored in the vibration and power flow calculations by assuming they play an insignificant role somehow due to the frequency range of interest, the coupling configurations, the idealized boundary conditions, the load conditions, etc. The effect of in-plane waves on the power flow is examined by Kessissoglou [25] by using a combination of a traveling wave and modal solution to describe the flexural and in-plane displacements. It is shown that in-plane waves can act as flanking paths for the flexural wave energy, especially as the frequency and distance from the source to the receiver increase. A substructure approach is presented by Wang et al. [26] to investigate the power flow characteristics of an L-shaped plate. Using the power flow density vector, they demonstrated that on the coupling edge of the L-shaped plate, energy does not always flow from the source to the receiver.

A common assumption made in all these analytical methods is that the plates in the coupled structures are restricted to being simply supported along opposite edges perpendicular to the coupling edge(s). Obviously, this condition imposes a serious limit to the applicability of these methods to many real-world plate structures in which a plate may be coupled with others along any edge(s) and the coupling conditions can be significantly different from the simply supported case. Often in dealing with a coupled plate system, the modal properties for each individual plate are first calculated by assuming the coupling edge(s) is free. The modal properties such obtained are subsequently used to determine the transfer functions (Green functions, or receptance functions) between the responses and the reaction forces (including moments) at the coupling edges in the actual system environment. Other limitations of the existing techniques include, for example, all the coupling edges that are parallel and of equal length.

In a previous study, an improved Fourier series method was proposed by Li [27] to determine the vibration of a single beam under arbitrary boundary conditions. This method is subsequently exploited to determine the vibration behaviors of two coupled beams [28], to investigate the effects of between-span couplings on the deflections of multi-span beam systems under moving loads [29], and to study the vibration of a rectangular plate with elastically restrained edges using the Rayleigh–Ritz method based on the products of beam functions [30]. Recently, the concept of using Fourier series to expand a solution is extended to two-dimensional problems, such as, for the in-plane [31] and out-of-plane [32] vibrations of plates with general elastic support. Unlike all the previous methods, the displacement solutions are *invariantly* expressed in the form of series expansions regardless of the boundary conditions. Based on the highest order of derivatives in the governing differential equation(s), the series is constructed in such a way that it can be directly differentiated, through term-by-term, to derive the series representations for other variables of interest such as bending moments and shearing forces. The unknown expansions coefficients are then obtained by letting the solution satisfy the governing equations and boundary conditions either exactly on a point-wise basis or approximately in a variational sense as in the Rayleigh–Ritz procedures. In the present study, this solution method is utilized to determine the vibration of two coupled plates with elastically restrained and coupled edges, which represents the most general case attempted so far. The layout of this paper is as follows. In Section 2, the analytical model for the two coupled plates is described for the general boundary and coupling conditions. Numerical examples are then discussed in Section 3. Finally, concluding remarks are made in Section 4.

2. Theoretical formulations

2.1. Descriptions for coupled plate structures

The coupled plate structure, consisting of plate 1 and plate 2, and the coordinate systems used in this investigation are shown in Fig. 1. The first plate (of length a_1, width b, and thickness h_1) lies in the x_1–y_1 plane. The boundary conditions for bending motion can be generally specified in terms of two kinds of restraining springs (translational and rotational) along each edge. Similarly, the general boundary conditions for in-plane vibrations can be described by another two sets of springs (normal and tangential) uniformly distributed along each edge in the x_1–y_1 plane. The units of the linear displacement and rotational spring stiffnesses for both bending and in-plane vibration components are N/m and Nm/rad for unit length. A list of the symbols is given in the Nomenclature.

Suppose that the second plate (of length a_2, width b, and thickness h_2) is connected to plate 1 at the common edge $x_1=0$ (or $x_2=a_2$). Plate 2 is also elastically restrained at the "free" edges. When the x_1–y_1–z_1 is chosen as the global coordinate system, the coupling angle θ alone is able to define the relative position between these two plates. At the structural junction, the effects of bending, out-of-plane shearing, in-plane longitudinal (normal to the coupling edge) and in-plane shearing (parallel with the coupling edge) will all be taken into account by including four types of coupling springs along the common edge, designated as K_c, k_{c1}, k_{c2}, and k_{c3}, respectively (see Fig. 1). The directions of the linear springs are defined in reference to the coordinate system attached to plate 1. The elastic supports at an edge represent a general set of boundary conditions; for instance, all the classical boundary conditions for both bending and in-plane vibrations can be readily simulated by setting each of the restraining springs to be infinitely rigid or soft. In the same way, different coupling conditions can be modeled by setting the coupling springs accordingly. Here, it should be pointed out that the term "soft" means that the coupling spring has extremely small stiffness coefficients, when they are set to zero in value, then the real free junction will be obtained.

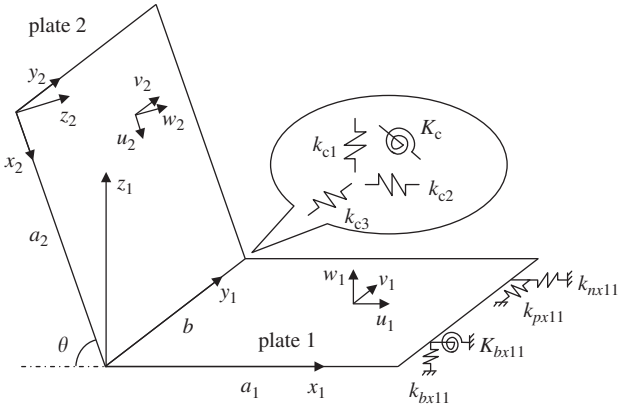

Fig. 1. Two rectangular plates coupled at a certain angle with general coupling and boundary conditions.

2.2. Series representations of the displacement functions

As previously done for a single plate [31,32], the transverse displacement will be expressed as

$$w_1(x_1,y_1)=\sum_{m=0}^{\infty}\sum_{n=0}^{\infty}A_{1mn}\cos\lambda_{a_1m}x_1\cos\lambda_{bn}y_1+\sum_{m=0}^{\infty}(a_{1m}\zeta_{1b}(y_1)+b_{1m}\zeta_{2b}(y_1)+c_{1m}\zeta_{3b}(y_1)+d_{1m}\zeta_{4b}(y_1))\cos\lambda_{a_1m}x_1$$
$$+\sum_{n=0}^{\infty}\left(e_{1n}\zeta_{1a_1}(x_1)+f_{1n}\zeta_{2a_1}(x_1)+g_{1n}\zeta_{3a_1}(x_1)+h_{1n}\zeta_{4a_1}(x_1)\right)\cos\lambda_{bn}y_1 \quad (1)$$

and the in-plane displacements as

$$u_1(x_1,y_1)=\sum_{m=0}^{\infty}\sum_{n=0}^{\infty}B_{1mn}\cos\lambda_{a_1m}x_1\cos\lambda_{bn}y_1+\sum_{m=0}^{\infty}(a_{in1m}\xi_{1b}(y_1)+b_{in1m}\xi_{2b}(y_1))\cos\lambda_{a_1m}x_1$$
$$+\sum_{n=0}^{\infty}\left(c_{in1n}\xi_{1a_1}(x_1)+d_{in1n}\xi_{2a_1}(x_1)\right)\cos\lambda_{bn}y_1, \quad (2)$$

and

$$v_1(x_1,y_1)=\sum_{m=0}^{\infty}\sum_{n=0}^{\infty}C_{1mn}\cos\lambda_{a_1m}x_1\cos\lambda_{bn}y_1+\sum_{m=0}^{\infty}(e_{in1m}\xi_{1b}(y_1)+f_{in1m}\xi_{2b}(y_1))\cos\lambda_{a_1m}x_1$$
$$+\sum_{n=0}^{\infty}\left(g_{in1n}\xi_{1a_1}(x_1)+h_{in1n}\xi_{2a_1}(x_1)\right)\cos\lambda_{bn}y_1, \quad (3)$$

where $\lambda_{a_1m}=m\pi/a_1$, $\lambda_{bn}=n\pi/b$, and the supplementary functions are defined in Appendix A. The introductions of these supplementary one-dimensional series are for the purpose of overcoming the discontinuity problems which the original displacement functions and their relevant derivatives will potentially encounter at the edges when they are periodically extended onto the entire x–y plane as implied mathematically by a two-dimensional Fourier series expansion. In the same way, the bending and in-plane displacements for plate 2 can be written out directly from the above equations by replacing subscript 1 with 2.

It is well known that when a function is expanded into Fourier series, it is *mathematically* viewed as a periodic function defined over the *entire* x–y plane. Consequently, if a plate is not "ideally" supported, the displacement function will potentially exhibit a discontinuity (or finite jump) along an edge and its Fourier series will only converge, if converge at all, to the mean values, rather than the correct boundary or coupling condition. The use of the supplementary functions is to ensure the *residual* displacement function *and* its relevant derivatives will not have any potential discontinuities along any edge. One can prove mathematically that the series given in Eq. (1) (or Eq. (2)) is able to expand and uniformly converge to *any* function $f(x_1, y_1)\in C^3$ (or $g(x_1, y_1)\in C^1$) for $\forall(x_1, y_1)\in D_1$: ($[0, a_1]\otimes[0, b_1]$). In addition, the series given in Eq. (1) (or Eq. (2)) can be simply differentiated, term-by-term, to obtain the uniformly convergent series expansions for up to the fourth-order (or second-order) derivatives in x_1 or y_1 direction. Thus, an *exact* transverse displacement solution can be obtained as a *particular* function $w_1(x_1, y_1)\in C^3$ for $\forall(x_1, y_1)\in D_1$ which satisfies the governing differential equation *exactly at every* field point and the boundary conditions *exactly at every* boundary point. By significantly improving the smoothness of the (residual) displacement function, the resulting Fourier series is ensured to uniformly converge fast, at least, at a speed of $(m\pi)^4$ for any boundary/coupling conditions [33,27].

By adopting the cosine series expansions given in Eqs. ((1)–(3)), one basically views the displacement functions as an even function of period $2a$ (and $2b$) in x (and y) direction. The displacement functions can also be expressed in the form of sine series expansion, implying that the displacement functions represent an odd function of period $2a$ (and $2b$) in x (and y) direction. For a general boundary condition, however, the cosine series tends to outperform the sine series in terms of the convergence rate [34]. If the displacements are considered as a periodic function of period a (and b) in x (and y) direction, they may then be expanded into a standard Fourier series with both sine and cosine terms. In such a case, however, the number of the supplementary functions will have to be doubled to ensure the smoothness of a displacement function and each of its derivatives along each boundary edge. Thus, the use of both sine and cosine terms offers no clear mathematical or numerical benefits for the problem of concern.

2.3. Solution for the coupled plate system

Once a suitable form of solutions has been established, the remaining task is to find such a set of expansion coefficients that the series will satisfy both the governing equations and the boundary/coupling conditions. In previous investigations for the single plate case, the series solutions are made to satisfy the governing equations and the boundary conditions *exactly on a point-wise basis* [31,32]. Such a solution process, however, tends to become cumbersome for general plate structures. Thus, the Rayleigh–Ritz procedure will be instead employed here.

The Lagrangian's function for the coupled plate system can be generally expressed as

$$L=T-V \quad (4)$$

where T denotes the total kinetic energy and V denotes the total potential energy.

For the two-plate system, the total kinetic and potential energies are given as

$$V = V_{1\text{bending}} + V_{1\text{in-}plane} + V_{2\text{bending}} + V_{2\text{in-}plane} + V_{\text{coupling}} \tag{5}$$

and

$$T = T_{1\text{bending}} + T_{1\text{in-}plane} + T_{2\text{bending}} + T_{2\text{in-}plane} \tag{6}$$

where $V_{j\text{bending}}$ (j=1, 2) represents the total potential energy associated with the bending vibration of the jth plate, including the strain energies and the potential energies stored in the bending-related boundary springs; $V_{j\text{in-plane}}$ indicates the total potential energy associated with the in-plane vibrations of the jth plate, including the strain energies due to the in-plane motions and potential energies stored in the in-plane-related boundary springs; $T_{j\text{bending}}$ and $T_{j\text{in-plane}}$ are the kinetic energies, respectively, corresponding to the bending and in-plane vibrations of the jth plate; and V_{coupling} denotes the potential energy associated with the coupling springs.

Take plate 1 for example. The potential and kinetic energies can be expressed as

$$\begin{aligned} V_{1\text{bending}} = {} & \frac{D_1}{2}\int_0^{a_1}\int_0^{b}\left\{\left(\frac{\partial^2 w_1}{\partial x_1^2}\right)^2+\left(\frac{\partial^2 w_1}{\partial y_1^2}\right)^2+2\mu_1\frac{\partial^2 w_1}{\partial x_1^2}\frac{\partial^2 w_1}{\partial y_1^2}+2(1-\mu_1)\left(\frac{\partial^2 w_1}{\partial x_1\partial y_1}\right)^2\right\}dx_1\,dy_1 \\ & +\frac{1}{2}\int_0^{b}\left[k_{bx10}w_1^2+K_{bx10}\left(\frac{\partial w_1}{\partial x_1}\right)^2\right]_{x_1=0}dy_1+\frac{1}{2}\int_0^{b}\left[k_{bx11}w_1^2+K_{bx11}\left(\frac{\partial w_1}{\partial x_1}\right)^2\right]_{x_1=a_1}dy_1 \\ & +\frac{1}{2}\int_0^{a_1}\left[k_{by10}w_1^2+K_{by10}\left(\frac{\partial w_1}{\partial y_1}\right)^2\right]_{y_1=0}dx_1+\frac{1}{2}\int_0^{a_1}\left[k_{by11}w_1^2+K_{by11}\left(\frac{\partial w_1}{\partial y_1}\right)^2\right]_{y_1=b}dx_1, \end{aligned} \tag{7}$$

$$T_{1\text{bending}} = \frac{1}{2}\int_0^{a_1}\int_0^{b}\rho_1 h_1\left(\frac{\partial w_1}{\partial t}\right)^2 dx_1\,dy_1 = \frac{1}{2}\rho_1 h_1\omega^2\int_0^{a_1}\int_0^{b} w_1^2\,dx_1\,dy_1, \tag{8}$$

$$\begin{aligned} V_{1\text{in-}plane} = {} & \frac{G_1}{2}\int_0^{a_1}\int_0^{b}\left\{\left(\frac{\partial u_1}{\partial x_1}+\frac{\partial v_1}{\partial y_1}\right)^2-2(1-\mu_1)\frac{\partial u_1}{\partial x_1}\frac{\partial v_1}{\partial y_1}+\frac{1-\mu_1}{2}\left(\frac{\partial v_1}{\partial x_1}+\frac{\partial u_1}{\partial y_1}\right)^2\right\}dx_1\,dy_1 \\ & +\frac{1}{2}\int_0^{b}\left[k_{nx10}u_1^2+k_{px10}v_1^2\right]_{x_1=0}dy_1+\frac{1}{2}\int_0^{b}\left[k_{nx11}u_1^2+k_{px11}v_1^2\right]_{x_1=a_1}dy_1 \\ & +\frac{1}{2}\int_0^{a_1}\left[k_{ny10}v_1^2+k_{py10}u_1^2\right]_{y_1=0}dx_1+\frac{1}{2}\int_0^{a_1}\left[k_{ny11}v_1^2+k_{py11}u_1^2\right]_{y_1=b}dx_1, \end{aligned} \tag{9}$$

and

$$T_{1\text{in-}plane} = \frac{1}{2}\int_0^{a_1}\int_0^{b}\rho_1 h_1\left[\left(\frac{\partial u_1}{\partial t}\right)^2+\left(\frac{\partial v_1}{\partial t}\right)^2\right]dx_1\,dy_1 = \frac{1}{2}\rho_1 h_1\omega^2\int_0^{a_1}\int_0^{b}(u_1^2+v_1^2)\,dx_1\,dy_1, \tag{10}$$

where w is the transverse displacement in the z-direction, u and v are the in-plane displacements in the x- and y-direction, respectively; ω is frequency in radians; D, G, μ, ρ, and h are, respectively, the flexible rigidity, the extensional rigidity, Poisson ratio, the mass density, and the thickness of the plate. The subscript 1 is used to indicate that all these variables are related to plate 1.

The in-plane modes mean the vibration resonance in the medium plane of the plate structure, compared to the flexural vibration which is normal to the plate plane. Although this component has little contribution to the noise radiation into ambient environment, it plays a significant role in the vibrational energy transmission. The in-plane vibration can be excited when there is a load component within or parallel to the plate, especially, in an L-shaped coupling plate structure, the transverse shear force in the source plate will directly excited the in-plane vibration in its receiving plate through the structural junction. Here, for an arbitrarily angled connection, the interactions are described by the potential energies stored in the four types of coupling springs:

$$\begin{aligned} V_{\text{coupling}} = {} & \frac{1}{2}\int_0^{b}[K_c(\partial w_1/\partial x_1|_{x_1=0}-\partial w_2/\partial x_2|_{x_2=a_2})^2+k_{c1}(w_1|_{x_1=0}-w_2|_{x_2=a_2}\cos\theta+u_2|_{x_2=a_2}\sin\theta)^2 \\ & +k_{c2}(u_1|_{x_1=0}-u_2|_{x_2=a_2}\cos\theta-w_2|_{x_2=a_2}\sin\theta)^2+k_{c3}(v_1|_{x_1=0}-v_2|_{x_2=a_2})^2]dy, \end{aligned} \tag{11}$$

where K_c, k_{c1}, k_{c2}, and k_{c3} denote the stiffnesses of the coupling springs (refer to Fig. 1 and the Nomenclature), and θ is the coupling angle between the two plates.

It should be noted that the contributions of the elastic restraints along boundary edges are included in Eqs. (7) and (9), and those of the coupling springs in Eq. (11). The stiffness for each of these elastic springs can be arbitrarily set as any value from zero to infinity. For simplicity, in this study the elastic support or coupling is assumed to be uniform along each edge. However, the current method can be readily applied to the most general boundary and coupling conditions in which the stiffness for each spring may vary with the spatial coordinates continuously, discontinuously or discretely. In such a case, the stiffnesses in Eqs. (7), (9), and (11) should be understood as functions of the spatial coordinates.

Substituting Eqs. ((5)–(11)) into (4) and minimizing the Lagrangian with respect to the all unknown Fourier coefficients, one is able to yield 38 sets of linear equations which can be written in a matrix form as

$$(\mathbf{K}-\omega^2\mathbf{M})\mathbf{E}=\mathbf{0}, \tag{12}$$

where **K** and **M** are, respectively, the stiffness and mass matrices for the coupled plate system, and **E** is a vector that contains all the unknown Fourier expansion coefficients in Eqs. ((1)–(3)). For conciseness, the definitions of these matrices and vector are given later in Appendix B.

The calculations of the surface and line integrals defined in Eqs. ((7)–(11)) usually represent the most time-consuming part of the work in finding the solution. In this study, all the integrations will be carried out analytically in a closed form. Thus, the computing time can be substantially reduced in comparison with a traditional numerical integration scheme. It is clear from Eq. (12) that the natural frequencies and the eigenvectors for the coupled plate system can now be easily obtained by solving a standard matrix eigenproblem. Each of the eigenvectors contains all the Fourier coefficients for the corresponding mode; its actual mode shape can be simply derived by substituting the Fourier coefficients into Eqs. ((1)–(3)). If the vibrational responses of the system to an applied load is desired, one just needs to include the work done by this load in the Lagrangian's function, which will eventually lead to a force term appearing on the right-hand side of Eq. (12). Once the vibrations are known on each plate, other variables of interest such as the power flows through the junction or/and its spatial distribution in the plates can be calculated easily, especially in view of the current analytical form of solutions.

The Rayleigh–Ritz solution is usually referred to as a weak or approximate solution, reflecting the fact that its smoothness requirement is typically relaxed. For instance, only the first derivatives of the flexural displacement function are required to be continuous throughout the solution domain in the Rayleigh–Ritz procedure in contrast to the third derivatives in the strong formulation. As mentioned earlier, however, the current displacement functions are adequately smooth so that the unknown expansion coefficients can be actually determined from the governing differential equations and the boundary/coupling conditions. It is well known mathematically that when the Rayleigh–Ritz solution is sufficiently smooth over the entire solution domain, it is actually equivalent to the exact solution derived from the strong formulation. By imposing a higher than necessary continuity requirement on the displacement functions, the series

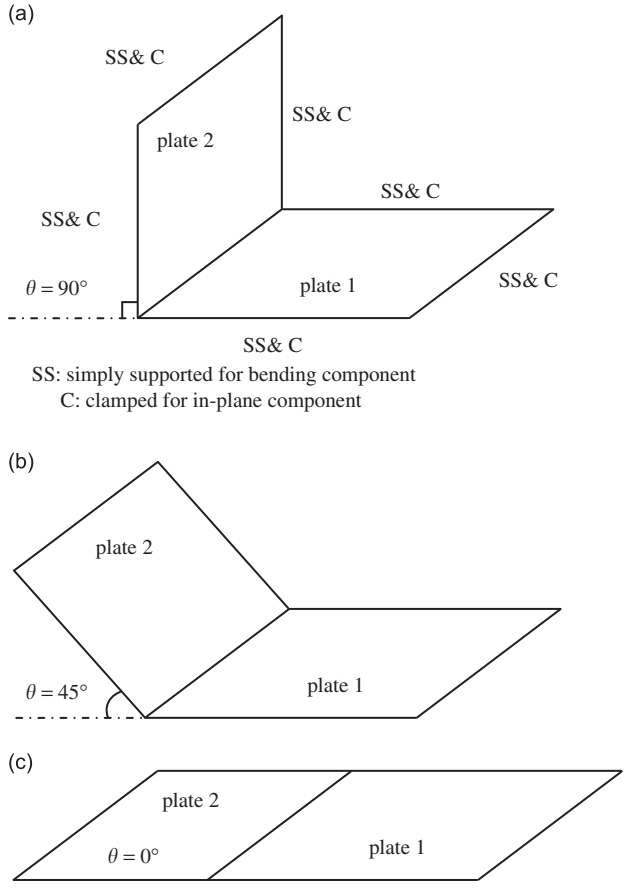

Fig. 2. Three coupling configurations with different angles at the structural junction.

expansions will be able to converge faster. More importantly, other variables of interest such as the bending moments, and in-plane and shear forces can be directly obtained from the displacement series through appropriate mathematical operations. In case if one does not care for such benefits, a traditional Rayleigh–Ritz solution can be calculated by

Table 1
Natural frequencies for an L-shaped plate structure with the coupling springs: $K_c=10^4$, $k_{c1}=10^4$, $k_{c2}=10^5$, and $k_{c3}=10^4$.

Mode no.	Natural frequencies (Hz)						
	$M=N=4$	$M=N=5$	$M=N=6$	$M=N=7$	$M=N=8$	$M=N=9$	FEA
1	16.243	16.205	16.179	16.165	16.154	16.147	16.109
2	20.573	20.539	20.480	20.468	20.444	20.438	20.389
3	34.065	34.037	33.813	33.805	33.713	33.710	33.553
4	52.600	52.576	52.271	52.264	52.139	52.136	51.934
5	57.465	57.326	57.323	57.275	57.274	57.251	57.209
6	60.491	60.246	60.240	60.160	60.158	60.122	60.061
7	70.519	70.117	69.917	69.793	69.715	69.659	69.445
8	77.413	76.868	76.683	76.522	76.442	76.373	76.125
9	97.868	96.734	96.535	96.196	96.112	95.965	95.583
10	116.66	114.87	114.79	114.23	114.21	113.96	113.49

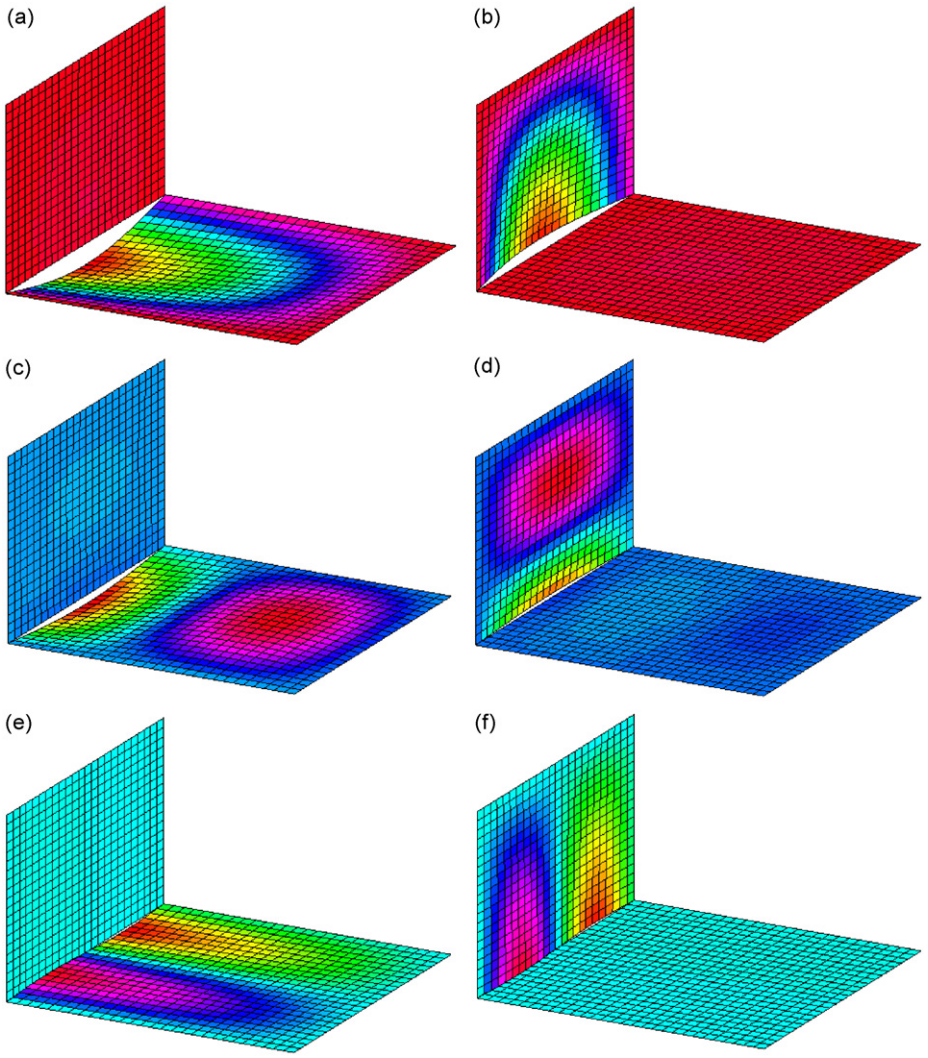

Fig. 3. The mode shapes for an elastically coupled L-shaped plate structure with the following coupling springs ($K_c=10^4$, $k_{c1}=10^4$, $k_{c2}=10^5$, and $k_{c3}=10^4$): (a) the first mode; (b) second; (c) third; (d) fourth; (e) fifth; (f) sixth.

simply dropping off the four terms with subscript 3 or 4 from Eq. (1), and all the supplementary terms from Eqs. (2) and (3).

For complex plate structures, the Rayleigh–Ritz procedure will have some advantages over those based on solving the governing equations and the boundary/coupling conditions directly. For example, they include: (a) all the unknown expansion coefficients can be obtained from the one-step solution process of minimizing the Lagrangian's function and (b)

Table 2
Natural frequencies for two rectangular plates rigidly coupled in an L-shaped configuration.

Mode no.	FEA (Hz)	Present (Hz)	Difference (%)
1	25.333	25.449	0.458
2	37.887	37.964	0.203
3	59.300	59.133	0.282
4	66.233	66.199	0.051
5	77.769	77.862	0.120
6	98.372	97.770	0.612
7	99.252	98.189	1.071
8	117.25	112.44	4.102
9	135.01	134.74	0.200
10	139.28	139.20	0.057

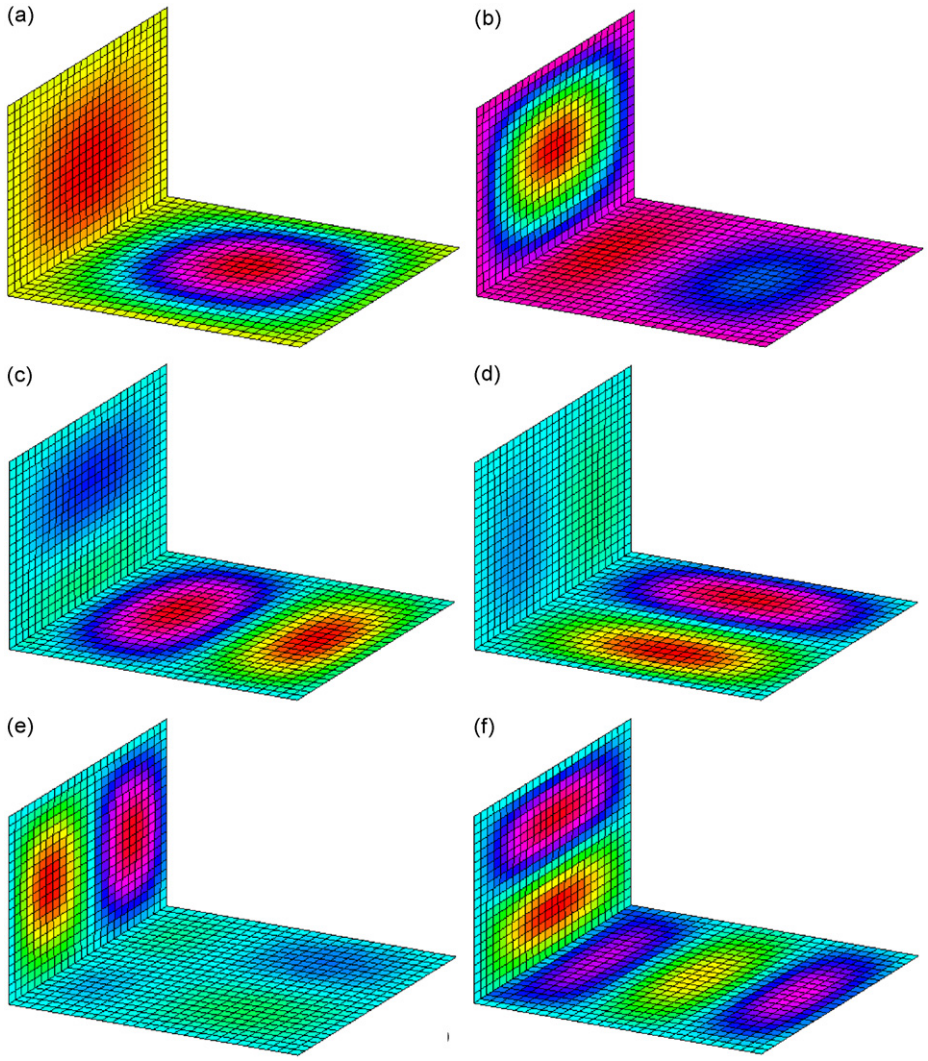

Fig. 4. The mode shapes for the rigidly coupled L-shaped plate structure: (a) the first mode; (b) second; (c) third; (d) fourth; (e) fifth; (f) sixth.

the effects of the couplings are limited to the neighboring plates (manifested in the banded coefficient matrices for the final system). The most important advantage, however, is perhaps related to the viability of developing an FEM-like assembly procedure for generating the final system by viewing each plate as an element. Although the current study is only focused on two coupled plates, it is quite straightforward to extend the proposed method to a complex structure composed of any number of plates.

3. Results and discussions

Several examples with different coupling configurations (see Fig. 2) will be considered in this section. Both plates are assumed to have the same thickness; that is, $h_1=h_2=0.008$ m. The lengths for plate 1 and 2 are $a_1=1.4$ m and $a_2=1.0$ m, respectively, and the width for the plates is $b=1.2$ m. The material properties for both plates are given as Young's modulus $E=2.16\times10^{11}$ N/m^2, mass density $\rho=7800$ kg/m^3, and Poisson ratio $\mu=0.28$.

As the first example, consider two plates connected together at a right angle to form an L-shaped plate structure as shown in Fig. 2(a). The simply supported and clamped boundary conditions are, respectively, specified for the flexural and in-plane displacements on plate 1 along the edges $y_1=0$, $x_1=a_1$, and $y_1=b$. The same boundary conditions are also applied to plate 2 along the corresponding edges. All the classical homogeneous boundary conditions (i.e., simply supported, clamped, and free) can be viewed as the special cases of the general elastic supports when each boundary spring becomes infinitely rigid or soft (the infinite stiffness is actually represented by a very large number, 5.0E+11, in the numerical calculations). The stiffness values of the coupling springs are arbitrarily chosen as $K_c=10^4$, $k_{c1}=10^4$, $k_{c2}=10^5$, and $k_{c3}=10^4$. Numerically, these values are close to the nominal bending rigidity of the plate, $Eh^3/12(1-\nu^2)=10^4$, a condition under which the elastic supports or joints tend to have significant impact to the dynamic characteristic of the plate(s). The first 10 natural frequencies of the coupled system are presented in Table 1 for different truncation schemes, $M=N=4, 5, 6, 7, 8, 9$. The FEA results obtained from an ANSYS model are also given there for comparison. In the FEA model, the element sizes are uniformly specified as 0.02 m $\times$ 0.02 m which is considered fine enough to accurately capture the spatial variations of these modes. It is seen that the current prediction compares well with the FEA results, and is sufficiently accurate even when only a small number of terms is included in the series expansions. In the subsequent calculations, for simplicity, all the series expansions will be truncated to $M=N=9$. Additionally, it is worthy to note that the current method is non-dimensional as shown in Eqs.((1)–(3)), then there will be no much difference in analyzing big or small size plates. However, the case is different for FEA. Since FEA is a grid-based method, the total mesh number will be considerably increased while the plate structure of large size is treated.

The corresponding mode shapes can be readily calculated by substituting the Fourier coefficients into the displacement expressions, Eqs. ((1)–(3)). Plotted in Fig. 3 are the first six modes for the L-shaped plate structure. It can be seen that due to the elastic coupling the displacements are no longer continuous across the junction. Now, consider these two plates are rigidly connected together. The condition of rigid connection can be easily simulated by setting the stiffness for each coupling spring to be infinitely large. The corresponding natural frequencies are given in Table 2 together with the FEA results. The first six modes are plotted in Fig. 4. In comparison with their counterparts in Fig. 3 for the elastic coupling case, not only have the displacement gaps disappeared at the junction, but also the activities tend to cover the entire structure. For the two plates connected at 90°, although out-of-plane displacements in two plates are not directly coupled through transverse shear force, they are still interacted through moment. As to the coupling between bending vibration in one plate

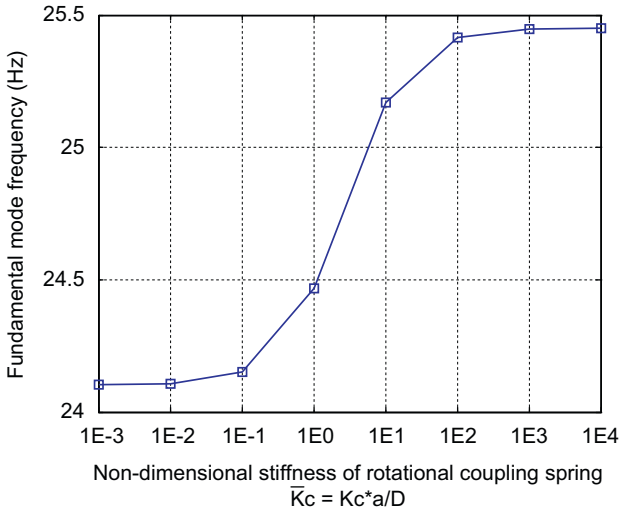

Fig. 5. Variation of the fundamental mode frequency of L-shaped plate with the non-dimensional rotational coupling spring stiffness $\overline{K}_c=K_ca/D$.

and the in-plane vibration in the other, the vertical coupling springs play a dominant role. For a very large case, corresponding to a rigid coupling such as the realistic welding joints, the interaction between bending and in-plane vibration is strong. And the displacements for both two vibration components are the same. For a soft case, namely, the stiffness coefficient is far smaller than the plate structural rigidity or zero, then the coupling between the bending and in-plane vibration is weak, and will cause the gap along the structural junction for a medium spring coefficient, which can be seen in Fig. 3.

Before proceeding another new coupling configuration, let us change the structural joint strength to study its effect on the modal characteristics of the L-shaped plate. Since there are various possible varying conditions of coupling springs, for simplicity, just the rotational spring K_c is considered to be changed, while the other three linear interface stiffnesses are all set as infinitely large numbers. The non-dimensional stiffness $\overline{K}_c = K_c a/D$ is defined and used here, in which $a=(a_1+a_2)/2$ and $D=Eh^3/12(1-\nu^2)$ is the flexural rigidity of plate structure. Fig. 5 illustrates the variation of fundamental modal frequencies with different rotational coupling conditions. It can be seen that when the non-dimensional rotational stiffness

Table 3
The first six modal frequencies of the L-shaped plate with various non-dimensional rotational coupling spring stiffness $\overline{K}_c = K_c a/D$.

Non-dimensional stiffness factor $\overline{K}_c$	Modal order					
	1	2	3	4	5	6
10^{-3}	24.104	33.852	54.473	65.409	75.323	93.360
10^{-2}	24.108	33.860	54.481	65.410	75.327	93.372
10^{-1}	24.151	33.945	54.556	65.425	75.364	93.493
10^{0}	24.466	34.648	55.197	65.547	75.686	94.478
10^{1}	25.170	36.804	57.544	65.949	76.927	96.962
10^{2}	25.417	37.823	58.925	66.167	77.734	97.690
10^{3}	25.448	37.962	59.129	66.199	77.860	97.769
10^{4}	25.451	37.976	59.151	66.202	77.873	97.777

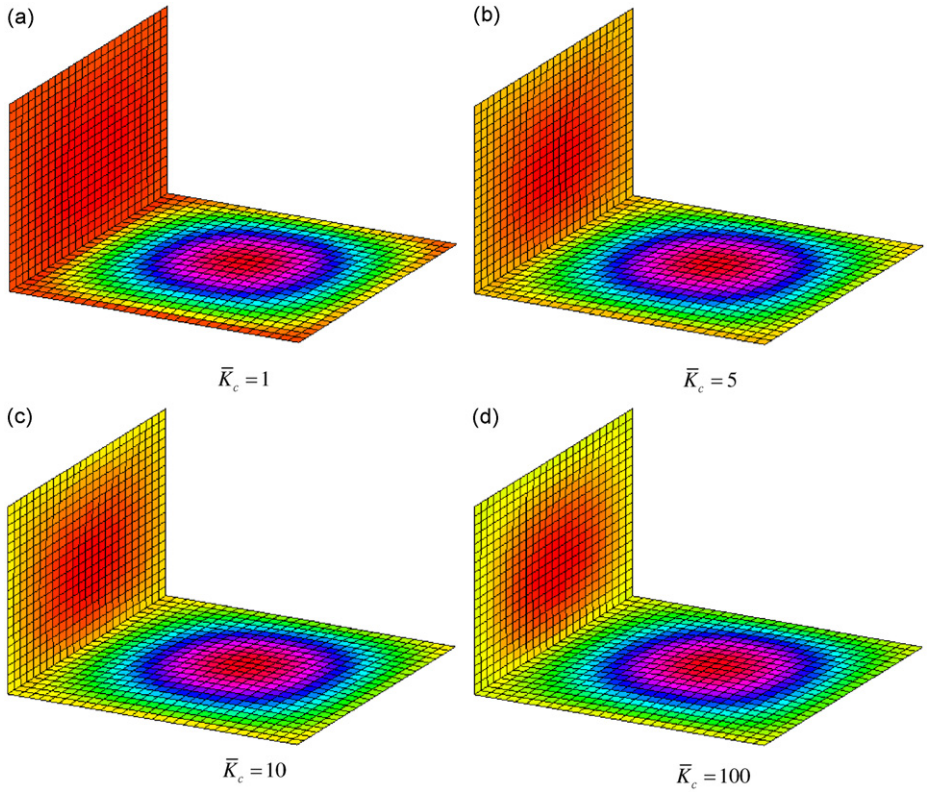

Fig. 6. Evolution of the fundamental mode shapes of the L-shaped plate with the variation of rotational interaction strength: (a) $\bar{K}_c$=1, (b) $\bar{K}_c$=5, (c) $\bar{K}_c$=10, (d) $\bar{K}_c$=100.

coefficient is smaller than 10^{-2}, its variation almost has no effect on modal parameters of the coupled plates. As the stiffness parameter further increases, a sensitive effect zone can be observed, in which the modal frequency increases with different rate depending on the coupling stiffness. When the coupling factor is beyond 10^3, the modal parameter approaches the upper limit basically corresponding to the rigid interaction case. Table 3 presents the frequency parameters of the first six modes under different coupling stiffness coefficients. Similar influence trend of the coupling conditions can be found for the other structural modes. In fact, this coupling stiffness effect behavior can be also understood by observing

Table 4
Natural frequencies for two plates coupled at 45° with the coupling springs: $K_c=10^6$, $k_{c1}=10^6$, $k_{c2}=10^5$, and $k_{c3}=10^4$.

Mode no.	ANSYS (Hz)	Present (Hz)	Difference (%)
1	5.9055	6.0115	1.795
2	7.2378	7.3628	1.727
3	15.174	15.030	0.949
4	24.776	25.387	2.466
5	30.762	30.801	0.127
6	33.386	33.600	0.641
7	43.272	42.889	0.885
8	45.940	45.744	0.427
9	54.783	55.751	1.767
10	67.973	69.752	2.617

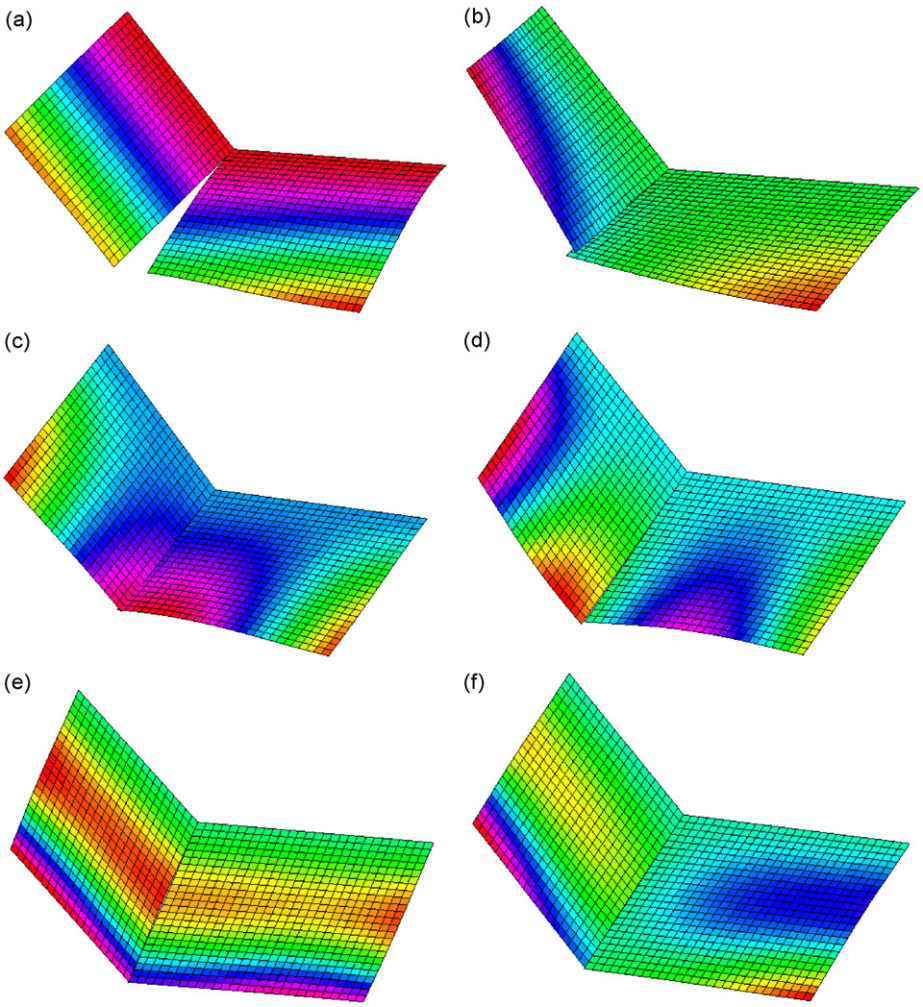

Fig. 7. The mode shapes for two plates elastically coupled at the angle of 45-degree with the following coupling springs ($K_c=10^6$, $K_{c1}=10^6$, $K_{c2}=10^5$, $K_{c3}=10^4$): (a) the first mode; (b) second; (c) third; (d) fourth; (e) fifth; (f) sixth.

the evolution of spatial distribution pattern of the coupled structural mode, as given in Fig. 6 for the fundamental mode cases. It is clearly shown that how the transfer from separate modes into a joined mode occurs within the coupling stiffness sensitive zone.

Now, change the coupling angle to 45° which corresponds to the second configuration shown in Fig. 2(b). In addition, the boundary conditions are modified; that is, both the flexural and in-plane displacements on each plate are now clamped at $y=b$, and all other edges are completely free. In Table 4, the first ten natural frequencies are presented for the elastic coupling condition: $K_c=10^6$, $k_{c1}=10^6$, $k_{c2}=10^5$, and $k_{c3}=10^4$. The first six modes are shown in Fig. 7. They clearly exhibit a global characteristic as compared with those modes given in Fig. 3 for the L-shaped case. When the coupling angle is different from 90°, the flexural vibrations on both plates will be directly coupled together through the transverse spring k_{c1}.

Lastly, a flat configuration as illustrated in Fig. 2(c) will be considered for both elastic and rigid coupling conditions. In this example, the boundary conditions will be changed back to the ones as previously specified for the L-shaped structure. When the coupling angle is equal to zero, the bending and in-plane vibrations will essentially become decoupled, and can be determined separately. For the elastic connection, the coupling springs are taken as $K_c=10^5$, $k_{c1}=10^5$, $k_{c2}=10^3$, and $k_{c3}=10^3$. In Table 5 the calculated natural frequencies are compared with those calculated from an ANSYS model. The first six mode shapes are plotted in Fig. 8. It is seen that the weak coupling actually allows the plates to move almost independently.

Table 5
Natural frequencies for the zero-angle coupled plate structure with the coupling springs: $K_c=10^5$, $k_{c1}=10^5$, $k_{c2}=10^3$, and $k_{c3}=10^3$.

Mode no.	ANSYS (Hz)	Present (Hz)	Difference (%)
1	16.965	16.996	0.183
2	21.228	21.275	0.221
3	36.011	36.131	0.333
4	54.290	54.470	0.332
5	57.922	57.956	0.059
6	60.438	60.498	0.099
7	72.836	73.021	0.254
8	77.250	77.475	0.004
9	97.034	97.395	0.372
10	115.52	115.95	0.372

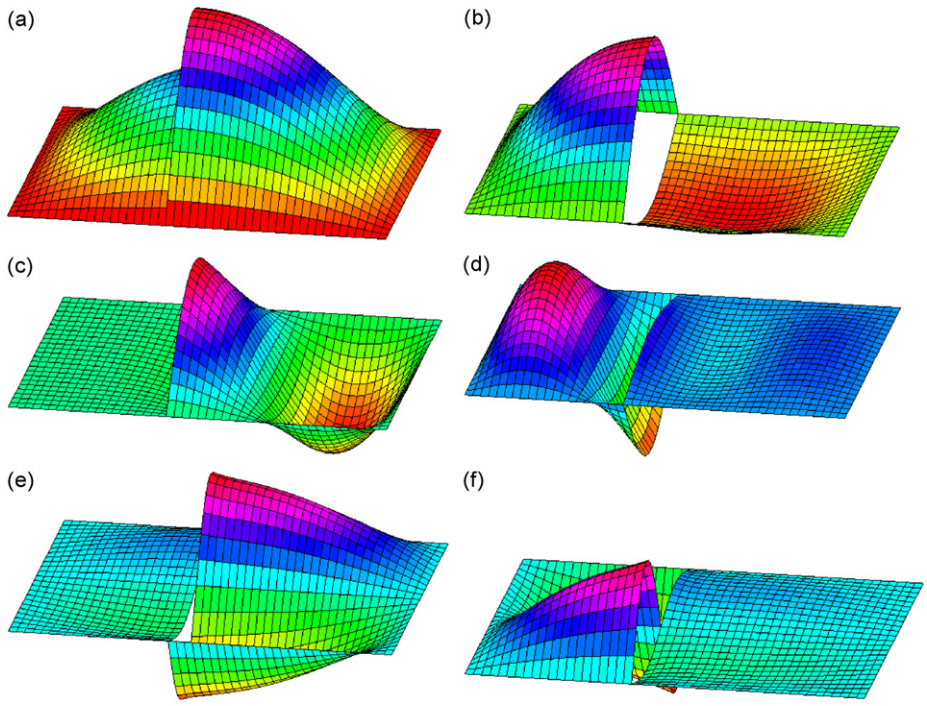

Fig. 8. The mode shapes for two plates elastically coupled in a flat configuration with the following coupling springs ($K_c=10^5$, $k_{c1}=10^5$, $k_{c2}=10^3$, and $k_{c3}=10^3$): (a) the first mode; (b) second; (c) third; (d) fourth; (e) fifth; (f) sixth.

Table 6
A comparison of the first 10 natural frequencies for the two plates rigidly coupled in a flat configuration.

Mode no.	Analytical (Hz)	Present (Hz)	Difference (%)
1	17.261	17.299	0.220
2	27.618	27.745	0.460
3	44.880	45.016	0.303
4	58.689	58.725	0.061
5	69.045	69.163	0.171
6	69.045	69.207	0.235
7	86.307	86.545	0.236
8	100.12	100.17	0.050
9	110.47	110.77	0.272
10	127.73	127.78	0.040

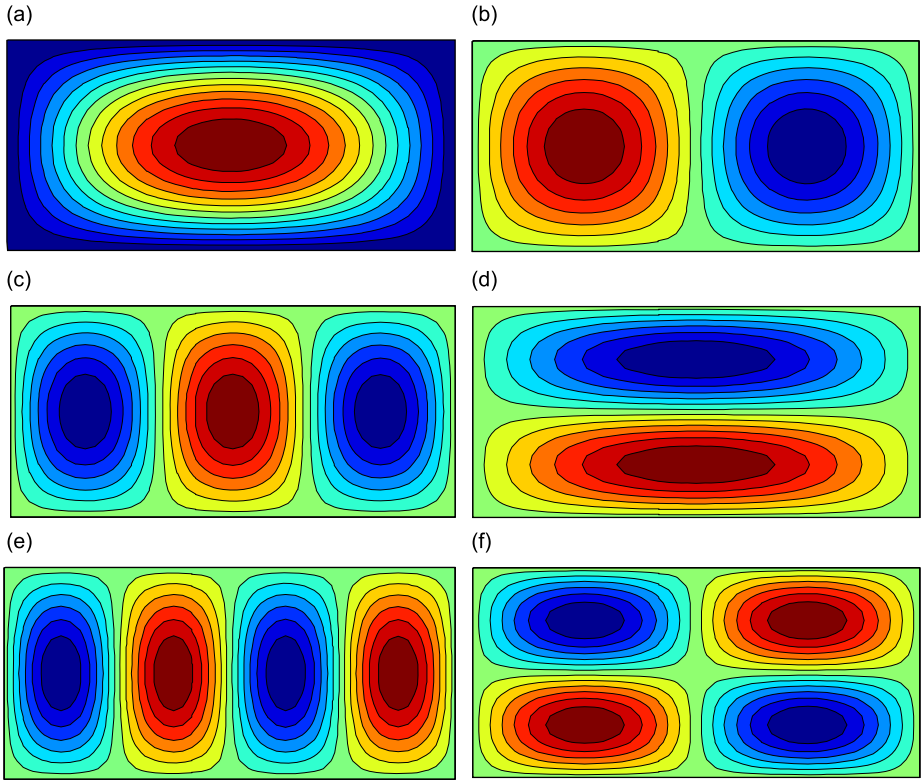

Fig. 9. The mode shapes for a rigidly coupled plate structure in a zero-degree configuration: (a) the first mode; (b) second; (c) third; (d) fourth; (e) fifth; (f) sixth.

The rigid connection condition is obtained simply by increasing stiffness values of the coupling springs to infinity. In this case, the two plate structure simply degenerates to a single plate, which has a combined length of a_1+a_2. Thus, the calculated natural frequencies and mode shapes can be directly compared with the analytical results for a single simply supported plate. A comparison of the natural frequencies is made in Table 6. The mode shapes for the first six modes are shown in Fig. 9. The minor differences for the calculated natural frequencies are believed due to the combination of the numerical truncation of the series expansions and the actual finiteness (instead of infinity) of the stiffness values for the boundary and coupling springs. This example, although it may appear to be trivial, has some very important implications; for instance, it says that a continuous plate component can be arbitrarily divided into a number of pieces to avoid non-uniformities/irregularities related to geometry or materials.

4. Conclusions

A general method is presented for the free vibration analysis of two rectangular plates elastically coupled together at an arbitrary angle. Instead of being simply supported along the edges perpendicular to the coupling edge as commonly

assumed in the literature, each plate can be generally restrained at any edge by a set of elastic springs of arbitrary stiffness. A universal set of series expressions is used to represent the transverse and in-plane displacements on each plate regardless of the boundary and coupling conditions. The unknown expansions coefficients are determined using the Rayleigh–Ritz method. Since the displacements functions represented by the series expansions are adequately smooth throughout the entire solution domain, the Rayleigh–Ritz solution is exact and mathematically equivalent to what is obtained from a strong formulation by directly solving the governing equations and the boundary and coupling conditions.

The accuracy and reliability of the proposed solution method have been illustrated through numerical examples which include various boundary conditions and coupling configurations. Compared to other solving technique such as FEA and other analytical solution, the following advantages may be drawn out: (1) no mesh is used, then there is no need for mesh refinement like the FEA does as the analysis frequency increases; (2) a fast convergence rate is observed, which implies that the efficient calculation can be achieved; (3) the current method does not involve much any modification to the solution algorithm or procedure when the boundary or coupling condition is changed. Even this study is focused on the free vibration of two coupled plates, the proposed method can be readily extended to structures consisting of any number of plates. The current model can also be used to investigate the effect of a boundary or coupling condition on the dynamic behavior of a built-up structure and on the power flows through any junctions and structural components.

Acknowledgement

The second author gratefully acknowledges the financial support from NSF Grant CMS-0528263.

Appendix A. Supplementary functions used in Eqs. ((1)–(3))

The supplementary functions used in the transverse displacement expression on plate 1 are defined as

$$\zeta_{1a_1}(x_1)=\frac{9a_1}{4\pi}\sin\left(\frac{\pi x_1}{2a_1}\right)-\frac{a_1}{12\pi}\sin\left(\frac{3\pi x_1}{2a_1}\right), \tag{A-1}$$

$$\zeta_{2a_1}(x_1)=-\frac{9a_1}{4\pi}\cos\left(\frac{\pi x_1}{2a_1}\right)-\frac{a_1}{12\pi}\cos\left(\frac{3\pi x_1}{2a_1}\right), \tag{A-2}$$

$$\zeta_{3a_1}(x_1)=\frac{a_1^3}{\pi^3}\sin\left(\frac{\pi x_1}{2a_1}\right)-\frac{a_1^3}{3\pi^3}\sin\left(\frac{3\pi x_1}{2a_1}\right), \tag{A-3}$$

$$\zeta_{4a_1}(x_1)=-\frac{a_1^3}{\pi^3}\cos\left(\frac{\pi x_1}{2a_1}\right)-\frac{a_1^3}{3\pi^3}\cos\left(\frac{3\pi x_1}{2a_1}\right), \tag{A-4}$$

$$\zeta_{1b}(y_1)=\frac{9b}{4\pi}\sin\left(\frac{\pi y_1}{2b}\right)-\frac{b}{12\pi}\sin\left(\frac{3\pi y_1}{2b}\right), \tag{A-5}$$

$$\zeta_{2b}(y_1)=-\frac{9b}{4\pi}\cos\left(\frac{\pi y_1}{2b}\right)-\frac{b}{12\pi}\cos\left(\frac{3\pi y_1}{2b}\right), \tag{A-6}$$

$$\zeta_{3b}(y_1)=\frac{b^3}{\pi^3}\sin\left(\frac{\pi y_1}{2b}\right)-\frac{b^3}{3\pi^3}\sin\left(\frac{3\pi y_1}{2b}\right) \tag{A-7}$$

and

$$\zeta_{4b}(y_1)=-\frac{b^3}{\pi^3}\cos\left(\frac{\pi y_1}{2b}\right)-\frac{b^3}{3\pi^3}\cos\left(\frac{3\pi y_1}{2b}\right). \tag{A-8}$$

It is easy to verify that

$$\zeta'_{1a_1}(0)=\zeta'_{2a_1}(a_1)=1, \tag{A-9}$$

$$\zeta'''_{3a_1}(0)=\zeta'''_{4a_1}(a_1)=1 \tag{A-10}$$

and all the other first and third derivatives are identically equal to zero at the edges.

Similar conditions holds for the y-related supplementary functions, $\zeta_{1b}(y_1)$, $\zeta_{2b}(y_1)$, $\zeta_{3b}(y_1)$, and $\zeta_{4b}(y_1)$.

The supplementary functions used in the in-plane displacement expansions on plate 1 are as follows:

$$\xi_{1a_1}(x_1)=x_1\left(\frac{x_1}{a_1}-1\right)^2, \quad \xi_{2a_1}(x_1)=\frac{x_1^2}{a_1}\left(\frac{x_1}{a_1}-1\right), \tag{A-11, 12}$$

$$\xi_{1b}(y_1)=y_1\left(\frac{y_1}{b}-1\right)^2, \text{ and } \xi_{2b}(y_1)=\frac{y_1^2}{b}\left(\frac{y_1}{b}-1\right). \tag{A-13, 14}$$

It is also easy to verify that

$$\xi'_{1a_1}(0)=1,\quad \xi_{1a}(0)=\xi_{1a}(a)=\xi'_{1a}(a)=0 \tag{A-15a, b}$$

and

$$\xi'_{2a}(a)=1,\text{ and }\xi_{2a}(0)=\xi_{2a}(a)=\xi'_{2a}(0)=0. \tag{A-16a, b}$$

Similar conditions holds for the y-related supplementary functions, $\zeta_{1b}(y_1)$ and $\zeta_{2b}(y_1)$.

Appendix B. Additional definitions

In Eq. (12), the unknown coefficient vector and the stiffness and mass matrices are defined as

$$\mathbf{E}=\begin{bmatrix}\mathbf{W}_1^{\mathrm{T}} & \mathbf{U}_1^{\mathrm{T}} & \mathbf{V}_1^{\mathrm{T}} & \mathbf{W}_2^{\mathrm{T}} & \mathbf{U}_2^{\mathrm{T}} & \mathbf{V}_2^{\mathrm{T}}\end{bmatrix}^{\mathrm{T}}, \tag{B-1}$$

$$\begin{aligned}\mathbf{W}_1=\{&A_{100},A_{101},\ldots,A_{1m'0},A_{1m'1},\ldots A_{1m'n'},\ldots,A_{1MN},a_{10},\ldots,a_{1M},b_{10},\ldots,b_{1M},\\ &c_{10},\ldots,c_{1M},d_{10},\ldots,d_{1M},e_{10},\ldots,e_{1N},f_{10},\ldots f_{1N},g_{10},\ldots,g_{1N},h_{10},\ldots,h_{1N}\}^{\mathrm{T}},\end{aligned} \tag{B-2}$$

$$\mathbf{U}_1=\left\{B_{100},B_{101},\ldots,B_{1m'0},B_{1m'1},\ldots B_{1m'n'},\ldots,B_{1MN},a_{in10},\ldots,a_{in1M},b_{in10},\ldots,b_{in1M},c_{in10},\ldots,c_{in1N},d_{in10},\ldots,d_{in1N}\right\}^{\mathrm{T}}, \tag{B-3}$$

$$\mathbf{V}_1=\left\{C_{100},C_{101},\ldots,C_{1m'0},C_{1m'1},\ldots C_{1m'n'},\ldots,C_{1MN},e_{in10},\ldots,e_{in1M},f_{in10},\ldots,f_{in1M},g_{in10},\ldots,g_{in1N},h_{in10},\ldots,h_{in1N}\right\}^{\mathrm{T}}, \tag{B-4}$$

$$\begin{aligned}\mathbf{W}_2=\{&A_{200},A_{201},\ldots,A_{2m'0},A_{2m'1},\ldots A_{2m'n'},\ldots,A_{2MN},a_{20},\ldots,a_{2M},b_{20},\ldots,b_{2M},\\ &c_{20},\ldots,c_{2M},d_{20},\ldots,d_{2M},e_{20},\ldots,e_{2N},f_{20},\ldots f_{2N},g_{20},\ldots,g_{2N},h_{20},\ldots,h_{2N}\}^{\mathrm{T}},\end{aligned} \tag{B-5}$$

$$\mathbf{U}_2=\left\{B_{200},B_{201},\ldots,B_{2m'0},B_{2m'1},\ldots B_{2m'n'},\ldots,B_{2MN},a_{in20},\ldots,a_{in2M},b_{in20},\ldots,b_{in2M},c_{in20},\ldots,c_{in2N},d_{in20},\ldots,d_{in2N}\right\}^{\mathrm{T}}, \tag{B-6}$$

$$\mathbf{V}_2=\left\{C_{200},C_{201},\ldots,C_{2m'0},C_{2m'1},\ldots C_{2m'n'},\ldots,C_{2MN},e_{in20},\ldots,e_{in2M},f_{in20},\ldots,f_{in2M},g_{in20},\ldots,g_{in2N},h_{in20},\ldots,h_{in2N}\right\}^{\mathrm{T}}, \tag{B-7}$$

$$\mathbf{K}=\begin{bmatrix}\mathbf{K}_{1-1} & \mathbf{K}_{1-2} & \mathbf{K}_{1-3} & \mathbf{K}_{1-4} & \cdots & \mathbf{K}_{1-38}\\ \mathbf{K}_{2-1} & \mathbf{K}_{2-2} & \mathbf{K}_{2-3} & \mathbf{K}_{2-4} & \cdots & \mathbf{K}_{2-38}\\ \mathbf{K}_{3-1} & \mathbf{K}_{3-2} & \mathbf{K}_{3-3} & \mathbf{K}_{3-4} & \cdots & \mathbf{K}_{3-38}\\ \mathbf{K}_{4-1} & \mathbf{K}_{4-2} & \mathbf{K}_{4-3} & \mathbf{K}_{4-4} & \cdots & \mathbf{K}_{4-38}\\ \vdots & \vdots & \vdots & \vdots & \ddots & \vdots\\ \mathbf{K}_{38-1} & \mathbf{K}_{38-2} & \mathbf{K}_{38-3} & \mathbf{K}_{38-4} & \cdots & \mathbf{K}_{38-38}\end{bmatrix} \tag{B-8}$$

and

$$\mathbf{M}=\begin{bmatrix}\mathbf{M}_{1-1} & \mathbf{M}_{1-2} & \mathbf{M}_{1-3} & \mathbf{M}_{1-4} & \cdots & \mathbf{M}_{1-38}\\ \mathbf{M}_{2-1} & \mathbf{M}_{2-2} & \mathbf{M}_{2-3} & \mathbf{M}_{2-4} & \cdots & \mathbf{M}_{2-38}\\ \mathbf{M}_{3-1} & \mathbf{M}_{3-2} & \mathbf{M}_{3-3} & \mathbf{M}_{3-4} & \cdots & \mathbf{M}_{3-38}\\ \mathbf{M}_{4-1} & \mathbf{M}_{4-2} & \mathbf{M}_{4-3} & \mathbf{M}_{4-4} & \cdots & \mathbf{M}_{4-38}\\ \vdots & \vdots & \vdots & \vdots & \ddots & \vdots\\ \mathbf{M}_{38-1} & \mathbf{M}_{38-2} & \mathbf{M}_{38-3} & \mathbf{M}_{38-4} & \cdots & \mathbf{M}_{38-38}\end{bmatrix}. \tag{B-9}$$

In the above equations, it has been assumed that all the series expansions are truncated to $m=M$ and $n=N$ for the sake of numerical calculations.

In order to demonstrate the structures of the coefficient matrices **K** and **M** in Eqs. (B–8) and (B–9), two new indices, $s=m(N+1)+n+1$ and $t=m'(N+1)+n'+1$, will be introduced to simplify the following notations. All the sub-matrices in the first row, which correspond to the derivatives of the Lagrangian with respect to A_{mn}, can be explicitly defined as follows:

$$\begin{aligned}\{K_{1-1}\}_{s,t}=&\int_0^{a_1}\int_0^{b}\Big\{D_1\lambda_{a_1m'}^2\lambda_{a_1m}^2\cos\lambda_{a_1m'}x_1\cos\lambda_{a_1m}x_1\cos\lambda_{bn'}y_1\cos\lambda_{bn}y_1+D_1\lambda_{bn'}^2\lambda_{bn}^2\cos\lambda_{a_1m'}x_1\cos\lambda_{a_1m}x_1\cos\lambda_{bn'}y_1\cos\lambda_{bn}y_1\\ &+D_1\mu_1\lambda_{bn'}^2\lambda_{a_1m}^2\cos\lambda_{a_1m'}x_1\cos\lambda_{a_1m}x_1\cos\lambda_{bn'}y_1\cos\lambda_{bn}y_1+D_1\mu_1\lambda_{a_1m'}^2\lambda_{bn}^2\cos\lambda_{a_1m'}x_1\cos\lambda_{a_1m}x_1\cos\lambda_{bn'}y_1\cos\lambda_{bn}y_1\\ &+D_12(1-\mu_1)\lambda_{a_1m'}\lambda_{bn'}\lambda_{a_1m}\lambda_{bn}\sin\lambda_{a_1m'}x_1\sin\lambda_{a_1m}x_1\sin\lambda_{bn'}y_1\sin\lambda_{bn}y_1\Big\}dx_1\,dy_1\\ &+[k_{bx10}+(-1)^{m'+m}k_{bx11}+k_{c1}]\int_0^{b}\cos\lambda_{bn'}y_1\cos\lambda_{bn}y_1\,dy_1+[k_{by10}+(-1)^{n'+n}k_{by11}]\int_0^{a_1}\cos\lambda_{a_1m'}x_1\cos\lambda_{a_1m}x_1\,dx_1,\end{aligned} \tag{B-10}$$

$$\{\mathbf{K}_{1-2}\}_{s,m'+1}=\int_0^{a_1}\int_0^b\Big\{D_1\lambda_{a_1m'}^2\lambda_{a_1m}^2\cos\lambda_{a_1m'}x_1\cos\lambda_{a_1m}x_1\zeta_{1b}(y_1)\cos\lambda_{bn}y_1-D_1\lambda_{bn}^2\cos\lambda_{a_1m'}x_1\cos\lambda_{a_1m}x_1\zeta''_{1b}(y_1)\cos\lambda_{bn}y_1$$
$$-D_1\mu_1\lambda_{a_1m}^2\cos\lambda_{a_1m'}x_1\cos\lambda_{a_1m}x_1\zeta''_{1b}(y_1)\cos\lambda_{bn}y_1+D_1\mu_1\lambda_{a_1m'}^2\lambda_{bn}^2\cos\lambda_{a_1m'}x_1\cos\lambda_{a_1m}x_1\zeta_{1b}(y_1)\cos\lambda_{bn}y_1$$
$$-D_12(1-\mu_1)\lambda_{a_1m'}\lambda_{a_1m}\lambda_{bn}\sin\lambda_{a_1m'}x_1\sin\lambda_{a_1m}x_1\zeta'_{1b}(y_1)\sin\lambda_{bn}y_1\Big\}dx_1\,dy_1$$
$$+\Big[k_{bx10}+(-1)^{m'+m}k_{bx11}+k_{c1}\Big]\int_0^b\zeta_{1b}(y_1)\cos\lambda_{bn}y_1\,dy_1+\big[k_{by10}\zeta_{1b}(0)+(-1)^nk_{by11}\zeta_{1b}(b)\big]\int_0^{a_1}\cos\lambda_{a_1m'}x_1\cos\lambda_{a_1m}x_1\,dx_1. \tag{B-11}$$

The sub-matrices, $\{\mathbf{K}_{1-3}\}_{s,m'+1}$, $\{\mathbf{K}_{1-4}\}_{s,m'+1}$, and $\{\mathbf{K}_{1-5}\}_{s,m'+1}$, can be directly obtained from Eq. (B-11) by replacing subscript 1 of the ζ-functions with 2, 3, and 4, respectively:

$$\{\mathbf{K}_{1-6}\}_{s,n'+1}=\int_0^{a_1}\int_0^b\Big\{-D_1\lambda_{a_1m}^2\zeta''_{1a_1}(x_1)\cos\lambda_{a_1m}x_1\cos\lambda_{bn'}y_1\cos\lambda_{bn}y_1$$
$$+D_1\lambda_{bn'}^2\lambda_{bn}^2\zeta_{1a_1}(x_1)\cos\lambda_{a_1m}x_1\cos\lambda_{bn'}y_1\cos\lambda_{bn}y_1+D_1\mu_1\lambda_{bn'}^2\lambda_{a_1m}^2\zeta_{1a_1}(x_1)\cos\lambda_{a_1m}x_1\cos\lambda_{bn'}y_1\cos\lambda_{bn}y_1$$
$$-D_1\mu_1\lambda_{bn}^2\zeta''_{1a_1}(x_1)\cos\lambda_{a_1m}x_1\cos\lambda_{bn'}y_1\cos\lambda_{bn}y_1-D_12(1-\mu_1)\lambda_{bn'}\lambda_{a_1m}\lambda_{bn}\zeta'_{1a_1}(x_1)\sin\lambda_{a_1m}x_1\sin\lambda_{bn'}y_1\sin\lambda_{bn}y_1\Big\}dx_1\,dy_1$$
$$+[k_{bx10}\zeta_{1a_1}(0)+(-1)^mk_{bx11}\zeta_{1a_1}(a_1)+k_{c1}\zeta_{1a_1}(0)]\int_0^b\cos\lambda_{bn'}y_1\cos\lambda_{bn}y_1\,dy_1+[k_{by10}+(-1)^{n'+n}k_{by11}]\int_0^{a_1}\zeta_{1a_1}(x_1)\cos\lambda_{a_1m}x_1\,dx_1. \tag{B-12}$$

Similarly, $\{\mathbf{K}_{1-7}\}_{s,n'+1}$, $\{\mathbf{K}_{1-8}\}_{s,n'+1}$, and $\{\mathbf{K}_{1-9}\}_{s,n'+1}$ can be obtained from Eq. (B-12) by replacing subscript 1 of the ζ-functions with 2, 3, and 4, respectively:

$$\{\mathbf{K}_{1-10}\}_{s,t}=0,\quad \{\mathbf{K}_{1-11}\}_{s,m'+1}=0,\quad \{\mathbf{K}_{1-12}\}_{s,m'+1}=0,\quad \{\mathbf{K}_{1-13}\}_{s,n'+1}=0,\quad \{\mathbf{K}_{1-14}\}_{s,n'+1}=0, \tag{B-13–17}$$

$$\{\mathbf{K}_{1-15}\}_{s,t}=0,\quad \{\mathbf{K}_{1-16}\}_{s,m'+1}=0,\quad \{\mathbf{K}_{1-17}\}_{s,m'+1}=0,\quad \{\mathbf{K}_{1-18}\}_{s,n'+1}=0,\quad \{\mathbf{K}_{1-19}\}_{s,n'+1}=0, \tag{B-18–22}$$

$$\{\mathbf{K}_{1-20}\}_{s,t}=(-1)^{m'+1}k_{c1}\cos\theta\int_0^b\cos\lambda_{bn'}y_2\cos\lambda_{bn}y_1\,dy \tag{B-23}$$

and

$$\{\mathbf{K}_{1-21}\}_{s,m'+1}=(-1)^{m'+1}k_{c1}\cos\theta\int_0^b\zeta_{1b}(y_2)\cos\lambda_{bn}y_1\,dy. \tag{B-24}$$

The sub-matrices $\{\mathbf{K}_{1-22}\}_{s,m'+1}$, $\{\mathbf{K}_{1-23}\}_{s,m'+1}$, and $\{\mathbf{K}_{1-24}\}_{s,m'+1}$ can be calculated from Eq. (B-24) by replacing subscript 1 of the ζ-functions with 2, 3, and 4, respectively:

$$\{\mathbf{K}_{1-25}\}_{s,n'+1}=-k_{c1}\cos\theta\zeta_{1a_2}(a_2)\int_0^b\cos\lambda_{bn'}y_2\cos\lambda_{bn}y_1\,dy. \tag{B-25}$$

The expressions for $\{\mathbf{K}_{1-26}\}_{s,n'+1}$, $\{\mathbf{K}_{1-27}\}_{s,n'+1}$ and $\{\mathbf{K}_{1-28}\}_{s,n'+1}$ can be obtained from Eq. (B-25) by replacing the subscript 1 of the ζ-functions with 2, 3 and 4, respectively:

$$\{\mathbf{K}_{1-29}\}_{s,t}=(-1)^{m'}k_{c1}\sin\theta\int_0^b\cos\lambda_{bn'}y_2\cos\lambda_{bn}y_1\,dy, \tag{B-26}$$

$$\{\mathbf{K}_{1-30}\}_{s,m'+1}=(-1)^{m'}k_{c1}\sin\theta\int_0^b\xi_{1b}(y_2)\cos\lambda_{bn}y_1\,dy, \tag{B-27}$$

$$\{\mathbf{K}_{1-31}\}_{s,m'+1}=(-1)^{m'}k_{c1}\sin\theta\int_0^b\xi_{2b}(y_2)\cos\lambda_{bn}y_1\,dy, \tag{B-28}$$

$$\{\mathbf{K}_{1-32}\}_{s,n'+1}=k_{c1}\sin\theta\xi_{1a_2}(a_2)\int_0^b\cos\lambda_{bn'}y_2\cos\lambda_{bn}y_1\,dy, \tag{B-29}$$

$$\{\mathbf{K}_{1-33}\}_{s,n'+1}=k_{c1}\sin\theta\xi_{2a_2}(a_2)\int_0^b\cos\lambda_{bn'}y_2\cos\lambda_{bn}y_1\,dy, \tag{B-30}$$

$$\{\mathbf{K}_{1-34}\}_{s,t}=0,\quad \{\mathbf{K}_{1-35}\}_{s,m'+1}=0,\quad \{\mathbf{K}_{1-36}\}_{s,m'+1}=0, \tag{B-31–33}$$

$$\{\mathbf{K}_{1-37}\}_{s,n'+1}=0,\text{ and }\{\mathbf{K}_{1-38}\}_{s,n'+1}=0. \tag{B-34, 35}$$

$$\{\mathbf{M}_{1-1}\}_{s,t}=\rho_1h_1\int_0^{a_1}\int_0^b\cos\lambda_{a_1m'}x_1\cos\lambda_{a_1m}x_1\cos\lambda_{bn'}y_1\cos\lambda_{bn}y_1\,dx_1\,dy_1, \tag{B-36}$$

and

$$\{\mathbf{M}_{1-2}\}_{s,m'+1} = \rho_1 h_1 \int_0^{a_1}\int_0^{b} \cos\lambda_{a_1 m'} x_1 \cos\lambda_{a_1 m} x_1 \zeta_{1b}(y_1)\cos\lambda_{bn} y_1 \, dx_1 \, dy_1. \tag{B-37}$$

The expressions for $\{\mathbf{M}_{1-3}\}_{s,m'+1}$, $\{\mathbf{M}_{1-4}\}_{s,m'+1}$, and $\{\mathbf{M}_{1-5}\}_{s,m'+1}$ can be obtained from Eq. (B-37) by replacing subscript 1 of the ζ-functions with 2, 3, and 4, respectively.

$$\{\mathbf{M}_{1-6}\}_{s,n'+1} = \rho_1 h_1 \int_0^{a_1}\int_0^{b} \zeta_{1a_1}(x_1)\cos\lambda_{a_1 m} x_1 \cos\lambda_{bn'} y_1 \cos\lambda_{bn} y_1 \, dx_1 \, dy_1. \tag{B-38}$$

The expressions for $\{\mathbf{M}_{1-7}\}_{s,n'+1}$, $\{\mathbf{M}_{1-8}\}_{s,n'+1}$, and $\{\mathbf{M}_{1-9}\}_{s,n'+1}$ can be obtained from Eq. (B-38) by replacing subscript 1 of the ζ-functions with 2, 3, and 4, respectively. The remaining sub-matrices, from $\{\mathbf{M}_{1-10}\}$ to $\{\mathbf{M}_{1-38}\}$, are all zero matrices.

References

[1] J.L. Guyader, C. Boisson, C. Lesueur, Energy transmission in finite coupled plates, part I: theory, *Journal of Sound and Vibration* 81 (1982) 81–92.
[2] J.M. Cuschieri, Structural power-flow analysis using a mobility approach of an L-shaped plate, *Journal of the Acoustical Society of America* 87 (1990) 1159–1165.
[3] M.D. McCollum, J.M. Cuschieri, Thick plate bending wave transmission using a mobility power flow approach, *Journal of the Acoustical Society of America* 88 (1990) 1472–1479.
[4] R.H. Lyon, In-plane contribution to structure noise transmission, *Noise Control Engineering Journal* 26 (1985) 22–27.
[5] A.N. Bercin, An assessment of the effects of in-plane vibrations on the energy flow between coupled plates, *Journal of Sound and Vibration* 191 (1996) 661–680.
[6] M.D. McCollum, J.M. Cuschieri, Bending and in-plane wave transmission in thick connected plates using statistical energy analysis, *Journal of the Acoustical Society of America* 88 (1990) 1480–1485.
[7] B.R. Mace, J. Rosenberg, The SEA of two coupled plates: an investigation into the effects of system irregularity, *Journal of Sound and Vibration* 212 (1999) 395–415.
[8] E.C.N. Wester, B.R. Mace, Statistical energy analysis of two edge-coupled rectangular plates: ensemble averages, *Journal of Sound and Vibration* 193 (1996) 793–822.
[9] R.M. Grice, R.J. Pinnington, Vibration analysis of a thin-plate box using a finite element model which accommodates only in-plane motion, *Journal of Sound and Vibration* 232 (2000) 449–471.
[10] S.A. Hambric, Power flow and mechanical intensity calculations in structural finite element analysis, *Journal of Vibration and Acoustics* 112 (1990) 542–549.
[11] B.R. Mace, P. Shorter, Energy flow models from finite element analysis, *Journal of Sound and Vibration* 233 (2000) 369–389.
[12] L. Cremer, M. Heckl, E.E. Ungar, *Structure-borne Sound*, 2nd ed, Springer, Berlin, 1988.
[13] P.G. Craven, B.M. Gibbs, Sound transmission and mode coupling at junctions of the plates, part I: representation of the problem, *Journal of Vibration and Acoustics* 77 (1981) 417–427.
[14] B.A.T. Petersson, C. Pierre, E.H. Dowell, Localization of vibrations by structural irregularity, *Journal of Vibration and Acoustics* 114 (1987) 549–564.
[15] A.C. Nilsson, Attenuation of structure-borne sound in superstructures on ships, *Journal of Sound and Vibration* 55 (1977) 71–91.
[16] R.S. Langley, Application of the dynamic stiffness method to the free and forced vibrations of aircraft panels, *Journal of Sound and Vibration* 135 (1989) 319–331.
[17] A.N. Bercin, R.S. Langley, Application of the dynamics stiffness technique to the in-plane vibration of plate structure, *Computers and Structures* 59 (1996) 869–875.
[18] J.A. Forrest, Mobility of plates structures modeling ship engine foundations, Proceeding of the Seventh International Congress on Sound and Vibration, 2000, pp. 1023–1030.
[19] J.M. Cuschieri, M.D. McCollum, In-plane and out-of-plane waves power transmission through L-plate junction using the mobility power flow approach, *Journal of the Acoustical Society of America* 100 (1996) 857–870.
[20] S. Azimi, J.F. Hamilton, W. Soedel, The receptance method applied to the free vibration of continuous rectangular plates, *Journal of Sound and Vibration* 93 (1984) 9–29.
[21] E.K. Dimitriadis, A.D. Pierce, Analytical solution for the power exchange between strongly coupled plates under random excitation: a test of statistical energy analysis concepts, *Journal of Sound and Vibration* 123 (1988) 397–412.
[22] N.H. Farag, J. Pan, On the free and forced vibration of single and coupled rectangular plates, *Journal of the Acoustical Society of America* 104 (1998) 204–216.
[23] H.S. Kim, H.J. Kang, J.S. Kim, Transmission of bending waves in inter-connected rectangular plates, *Journal of the Acoustical Society of America* 96 (1994) 1557–1562.
[24] M. Beshara, A.J. Keane, Vibrational energy flows between plates with compliant and dissipative couplings, *Journal of Sound and Vibration* 213 (1998) 511–535.
[25] N.J. Kessissoglou, Power transmission in L-shaped plates including flexural and in-plane vibration, *Journal of the Acoustical Society of America* 115 (2004) 1157–1169.
[26] Z.H. Wang, J.T. Xing, W.G. Price, An investigation of power flow characteristics of L-shaped plates adopting a substructure approach, *Journal of Sound and Vibration* 250 (2002) 627–648.
[27] W.L. Li, Free vibrations of beams with general boundary conditions, *Journal of Sound and Vibration* 237 (2000) 709–725.
[28] W.L. Li, M.W. Bonilha, J. Xiao, Vibrations and power flows in a coupled beam system, *Journal of Vibration and Acoustics* 129 (2007) 616–622.
[29] H.A. Xu, W.L. Li, Dynamic behavior of multi-span bridges under moving loads with focusing on the effect of the coupling conditions between spans, *Journal of Sound and Vibration* 312 (2008) 736–753.
[30] W.L. Li, Vibration analysis of rectangular plates with general elastic boundary supports, *Journal of Sound and Vibration* 273 (2004) 619–635.
[31] J.T. Du, W.L. Li, G.Y. Jin, T.J. Yang, Z.G. Liu, An analytical method for the in-plane vibration analysis of rectangular plates with elastically restrained edges, *Journal of Sound and Vibration* 306 (2007) 908–927.
[32] W.L. Li, X.F. Zhang, J.T. Du, Z.G. Liu, An exact series solution for the transverse vibration of rectangular plates with general elastic boundary supports, *Journal of Sound and Vibration* 321 (2009) 254–269.
[33] G.P. Tolstov, *Fourier Series*, Prentice-Hall, Englewood Cliffs, NJ, 1965.
[34] W.L. Li, Comparison of Fourier sine and cosine series expansions for beams with arbitrary boundary conditions, *Journal of Sound and Vibration* 255 (2002) 185–194.